Research Article | Vol. 33, No. 25 / 15 Dec 2025 / Optics Express 53329

Optics EXPRESS

Inherent optical properties of *Phaeocystis globosa* colonies in the China Seas

XUE LI,[1,2] SHAOLING SHANG,[1,*] ZHONGPING LEE,[1] BANGYI TAO,[3] YUE GAO,[1] ZHANGXI HU,[4] DONGMEI LIAN,[1] AND GONG LIN[1]

[1]*State Key Laboratory of Marine Environmental Science, College of Ocean and Earth Sciences, Xiamen University, Xiamen 361102, China*
[2]*Jiangsu Institute of Marine Resources Development, Jiangsu Ocean University, Lianyungang 222005, China*
[3]*State Key Laboratory of Satellite Ocean Environment Dynamics, Second Institute of Oceanography, Ministry of Natural Resources, Hangzhou 310012, China*
[4]*College of Fisheries, Guangdong Provincial Key Laboratory of Aquatic Animal Disease Control and Healthy Culture, Laboratory of Marine Ecology and Aquaculture Environment of Zhanjiang, Guangdong Ocean University, Zhanjiang 524088, China*
[*]*slshang@xmu.edu.cn*

Abstract: *Phaeocystis globosa* (*P. globosa*), a distinctive harmful algal bloom (HAB)-forming species, is capable of alternating between free-living cells and gelatinous colonies. Developing optical techniques for the rapid detection of this HAB-causing species requires knowledge of its inherent optical properties (IOPs), particularly in the form of intact colonies. However, these properties remain poorly understood for the giant colonies of *P. globosa*, given that measurements of them are challenging. Here, by modifying existing methods for IOPs measurements, we successfully obtained the absorption and scattering coefficients of intact *P. globosa* colonies up to 25 mm in size. Six strains were isolated from different regions of the China Seas: one collected *in situ*, and the others grown in culture. Our results show that the IOPs of intact colonies are similar to those of free-living cells, regardless of colony size (1–25 mm). A prominent absorption peak at 468–472 nm was consistently observed across all five colonial strains and the free-living cell strain, corresponding to chlorophyll-c_3 (Chl-c_3) absorption. Notably, although intracolonial fluid contains colored dissolved organic matter and the colony envelope consists of optically active particulate matter, their contributions to light absorption and scattering by colonies in the spectral range of 400-750 nm are negligible when the colony remains non-collapsed. Interestingly, broken colonies exhibit reduced chlorophyll-specific absorption compared to intact ones, suggesting that colony structure enhances light absorption. This result, combined with the fact that measurements of broken colonies via the traditional quantitative filter technique are compromised by uneven pad distribution, underscores the importance of measuring IOPs in intact *P. globosa* colonies rather than in filtered samples containing broken colonies. These findings will undoubtedly aid in the future development of bio-optical models for *P. globosa* colonies and enhance remote sensing algorithms for detecting *P. globosa* blooms.

1. Introduction

Phaeocystis, a genus of eurythermal and euryhaline phytoplankton, is found in waters ranging from polar to tropical regions and plays a crucial role in marine primary production, carbon and sulfur biogeochemical cycles, food web structures, and global climate change [1–3]. *Phaeocystis globosa* (*P. globosa*) is one of the 10 known *Phaeocystis* species that exhibits a complex polymorphic life cycle. Normally, it exists as free cells (3–9 µm in size), but forms gelatinous colonies (10 µm–3 cm in size) during blooms [4,5]. The colonies are spherical in shape,

#576459 https://doi.org/10.1364/OE.576459
Journal © 2025 Received 15 Aug 2025; revised 27 Oct 2025; accepted 14 Nov 2025; published 11 Dec 2025

Optics EXPRESS

comprising thousands to millions of *P. globosa* cells along with intracolonial liquid, all enclosed by a mucous envelope [1,2]. The envelope is an exopolysaccharide matrix tegument [1], while the intracolonial fluid contains dissolved organic matter; the concentration of dissolved organic carbon in this fluid is up to 25 times higher than ambient levels, as reported in a study on giant colonies in Vietnam's coastal waters [3]. Harmful algal blooms (HABs) of *P. globosa* frequently occur in European, Vietnamese, and Chinese coastal waters [4–8]. Blooms of *P. globosa* cause the death of benthic organisms, fish, shrimp, and shellfish [9,10], and severely damage aquatic ecosystems as well as tourism [1,11,12]. Furthermore, colonies may clog water intake sieves, posing serious risks to nuclear power plant operation [12,13]. These issues have raised widespread concerns and highlighted the need for efficient identification and monitoring of *P. globosa* blooms [4,5].

In the China Seas, the first *P. globosa* bloom event was recorded in 1997 [14]. Since then, it has transitioned from being a newly recorded algal bloom to becoming a typical algal bloom species, with over 100 outbreaks documented in coastal waters by 2023 [15]. Various strains of *P. globosa*, which differ in pigments, have been documented in the China Seas [16]. Notably, *P. globosa* colonies in the China Seas are large, with diameters reaching up to 3 cm—comparable to the giant colonies found in Vietnam coastal waters—whereas those in European waters measure only a few millimeters across [4,5].

Traditional methods for identifying and tracing *P. globosa* blooms rely on *in situ* moored measurements and laboratory techniques, such as microscopy, flow cytometry, genetic analysis, and high-performance liquid chromatography (HPLC) [12,17–19]. These techniques are highly accurate for taxonomic identification but are restricted by their discrete and labor-intensive sampling nature, making them unsuitable for continuous and/or synoptic observations over large spatial and temporal scales. In contrast, satellite remote sensing provides broad, frequent coverage that enables effective monitoring of bloom dynamics. Various remote-sensing methods have been developed to detect *P. globosa* blooms. For tiny *P. globosa* colonies in Europe, multispectral and hyperspectral techniques have been proposed based on laboratory experiments and field observations in the eastern English Channel and the southern North Sea [10,11]. A multivariate classifier was developed to detect *Karenia mikimotoi* and *P. globosa* blooms from ocean color images [20]. Recently, Lavigne et al. [21] successfully applied two existing *P. globosa* detection algorithms by deploying an autonomous hyperspectral radiometer system in Belgian coastal waters. For giant *P. globosa* colonies in the China Seas, Li et al. [13] proposed a criterion to discriminate *P. globosa* from diatoms based on the remote sensing reflectance (R_{rs}, sr^{-1}) measured *in situ*, and attempted an empirical approach to quantify *P. globosa* biomass based on hyperspectral R_{rs} measurements via an unmanned aerial vehicle. Several additional empirical studies using multispectral satellite ocean color measurements have recently been conducted to support the monitoring of *P. globosa* blooms in the China Seas [22–24]. Although considerable success in detecting and mapping *P. globosa* blooms have been achieved using these remote-sensing approaches, none of these algorithms are grounded in the inherent optical properties (IOPs) of intact *P. globosa* colonies or in subsequent reflectance modeling. In particular, the IOPs of *P. globosa* in the form of intact giant colonies, including absorption and scattering properties, remain entirely unknown, since traditional methods and commercial devices for IOPs measurements are difficult to apply to giant gelatinous *P. globosa* colonies (see details in Section 2). Acquiring knowledge of the IOPs of intact colonies is extremely important, as this is crucial for advancing the development of remote sensing algorithms designed to detect and quantify *P. globosa* blooms. Note that optical sensors, whether mounted on satellites, UAVs, or ships, receive signals in the form of R_{rs}, which is determined by the *in situ* absorption and backscattering coefficients of intact colonies, rather than those of filtered broken colonies.

To acquire knowledge of the IOPs of intact colonies, especially natural giant colonies, in this study, we collected six strains of *P. globosa* from the China Seas and characterized their IOPs by

Optics EXPRESS

modifying existing methods. Since the colonies consist of abundant *P. globosa* cells, intracolonial fluid containing dissolved organic matter, and an envelope, we propose two hypotheses. First, the IOPs of intact colonies differ from those of free-living cells, given that some dissolved organic matter is potentially colored and the envelope is a light-active particulate substance. Second, the IOPs of intact colonies is the same as those of broken colonies, if they are measured using the same method.

By characterizing the IOPs of *P. globosa* colonies in their natural state, the species-specific bio-optical models and remote sensing algorithms can be refined to accurately map the spatial extent and intensity of blooms caused by this unique harmful algal species. This, in turn, will support deeper insights into the biogeochemical and ecological processes linked to such blooms. Moreover, this work on measuring the IOPs of large *P. globosa* colonies while preserving their structural integrity will certainly be of value for bio-optical research on other similar algal species.

2. Materials and methods

2.1. P. globosa samples

The *P. globosa* samples used in this study included one strain from *in situ* surveys and five strains from cultures. The *in situ* strain (PG-*in-situ*) (Fig. 1(a)), was collected from Dapeng Bay in Guangdong Province and placed under indoor cultural conditions for measurements on the following day. Five cultured strains were obtained from the Center for Collections of Marine Algae, Xiamen University, and the Institute of Oceanology, Chinese Academy of Sciences (Table 1 and Fig. 1(b)-(e)). The cultural strains were cultured in cell and tissue culture flasks (Jet BIOFIL, Ltd.), with 0.22 μm filtered and sterilized seawater supplemented with L1 medium. The cultures were maintained at 20 ± 2 °C under 2400 ± 200 lx irradiance with a 14:10 h light-dark photoperiod.

The six strains of *P. globosa* as shown in Fig. 1 and Table 1 exhibited similarities and differences in their morphology, isolated sites, and sources. PG-*in-situ* is the only wild strain, with colonies reaching sizes of over 20 mm. CCMA-124 consists solely of free-living cells and does not form colonies. Among the colony samples, CCMA-115 was the tiniest, with a mean diameter of 1 mm, whereas CCMA-166 was the largest, exceeding 25 mm in diameter.

2.2. Measurements

2.2.1. Absorption

Absorption meters such as AC-S/AC9 (WET Labs Inc.), integrating cavity absorption meter (ICAM, Turner Designs, Inc.), and point-source integrating-cavity absorption meter (OSCAR, TriOS, Inc.) are widely used *in situ*. However, giant gelatinous colonies with mucilage cannot completely pass through the pipelines (maximum diameter: 0.95 cm), leading to broken colonies or pump clogging [25].

The most commonly utilized approach for particle absorption measurements is the quantitative filter technique (QFT) [26,27]. QFT requires pads to filter water samples. The filtration process disrupts the shape and internal structure of the colonies, making it impossible to determine the absorption properties of intact colonies. On the other hand, the filtration process leads to an uneven distribution of cells and broken envelopes on the filters (Fig. 2(a)). This issue is particularly severe in field-collected colony samples, as they possess a tougher and more elastic outer envelope compared to colonies cultured indoors [28–29]. The issue of uneven distribution can be mitigated by thoroughly and physically disrupting the colony samples prior to filtration, making it possible to separately quantify the absorption of *P. globosa* cells, the colonial envelope, and intracolonial fluid, and then to combine these to derive the total absorption of broken colonies.

We therefore employed the internal sphere mode (IS-mode) of QFT for particle absorption measurements, following the method described by Röttgers and Gehnke [30]. The dual-beam

Optics EXPRESS

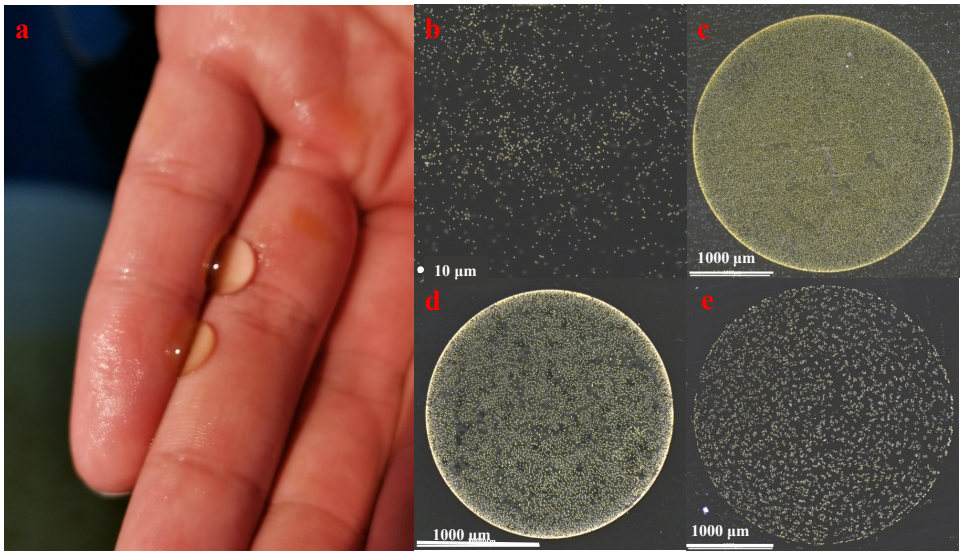

Fig. 1. (a) Photograph of *P. globosa* colonies (PG-*in-situ*) collected in Dapeng Bay; (b)-(e) micrographs of CCMA-124, CCMA-166, PG-2015, and PG-2021, respectively.

Table 1. Information on six *P. globosa* strains isolated from the China Seas

Name of strains	Morphology	Isolated site	Maximum diameter of colonies	Source of algae
CCMA-124	free-living cells	Beibu Gulf, China	—	Xiamen University (Culture)
CCMA-115	free-living cells and tiny gelatinous colonies	Beibu Gulf, China	mean 1 mm	Xiamen University (Culture)
CCMA-166	free-living cells and gelatinous colonies	Beibu Gulf, China	> 25 mm	Xiamen University (Culture)
PG-2015	free-living cells and gelatinous colonies	Qinzhou Bay, China	> 15 mm	Institute of Oceanology, Chinese Academy of Sciences (Culture)
PG-2021	free-living cells and gelatinous colonies	Dapeng Bay, China	> 5 mm	Xiamen University (Culture)
PG-*in-situ*	free-living cells and gelatinous colonies	Dapeng Bay, China	> 20 mm	*in situ*

Optics EXPRESS

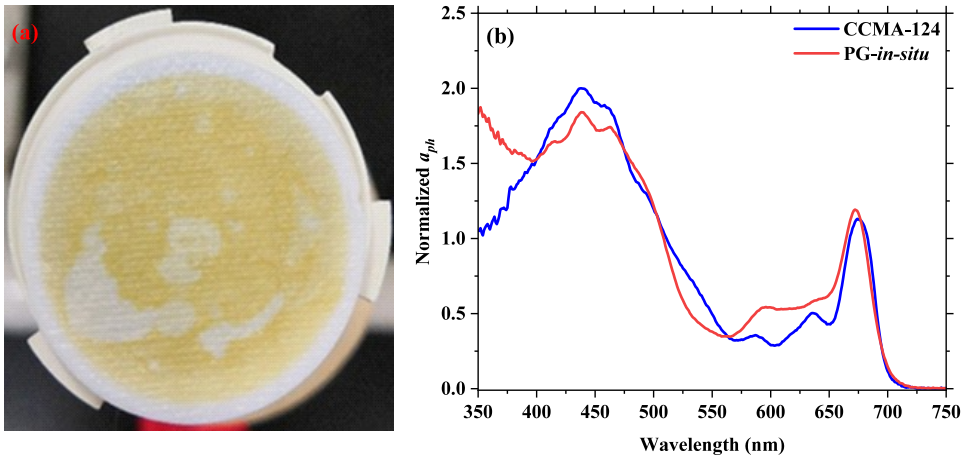

Fig. 2. (a) An example of unevenly distributed particles (including *P. globosa* cells and broken envelopes) on the filter pad; (b) phytoplankton absorption coefficient (a_{ph}) as measured by QFT, with the blue curve representing CCMA-124 (free-living cell sample) and the red curve representing PG-*in-situ* (field-collected colony sample, 25 mm in diameter).

PerkinElmer (PE) Lambda 950 spectrophotometer, equipped with a 150 mm diameter integrating sphere, was used. Note that the CCMA-124 sample (free-living cell) was filtered according to the IOCCG Protocol [31], while other colony samples were physically broken up before filtration to facilitate filtration and improve uniformity on filter pads for subsequent measurements. Afterwards, the Whatman GF/F filter pads containing the samples were placed at the center of an integrating sphere using a holder designed for the PE950. The absorbance of the sample relative to a blank filter pad was measured to obtain the optical density of particulate matter (OD_p). The filter pad was then returned to the filtration system, where methanol was added, and the sample was immersed for 1 h to remove the phytoplankton pigments. After rinsing the filter pad with approximately 50 mL of pure water, the optical density was measured again to determine the non-algal absorption (OD_d). The particulate absorption coefficient (a_p, m^{-1}) was calculated using the equation provided in Röttgers and Gehnke [30]:

$$a_p(\lambda) = \frac{2.303 \times S}{V_f} \times 0.323 \times OD_P^{1.0867} \tag{1}$$

Here, S refers to the actual area occupied by particles on the filter pad (m^2) and V_f is the volume of the filtered water sample (m^3). Similarly, the absorption coefficient of non-algal particles (a_d) was also calculated, and the absorption coefficient of phytoplankton pigments (a_{ph}) was the difference between a_p and a_d, i.e. $a_{ph}(\lambda) = a_p(\lambda) - a_d(\lambda)$.

Meanwhile, colony samples were physically broken up and then filtered using the 0.2 µm PC Millipore filters. The absorption of the colored dissolved organic matter (CDOM, a_g) in the filtrate was measured according to the Ocean Optics Protocols Version 2.0 [32]. By combining these two components- $a_p(a_{ph} + a_d)$, and a_g -the total absorption of broken colonies excluding the contribution from pure water (hereafter referred to as a_{c_w}) was thus obtained.

To enable absorption measurements of *P. globosa* colonies while preserving their original structural integrity, we chose the method for measuring the absorption of suspension samples using an integrating sphere with a central cuvette system (CIS) [33–35]. By placing the sample cuvette in the center of an integrating sphere to capture laterally scattered and backscattered light, this system enhances absorption measurements [34]. The CIS method exhibits a measurement accuracy comparable to commercial absorption meters, such as the point-source integrating-cavity

Optics EXPRESS

absorption meter [33]. Utilizing longer pathlength cuvettes in the CIS method can enhance the signal-to-noise ratio and potentially reduce most errors associated with QFT [33]. A centrally mounted sample holder and a 4-cm-pathlength cylindrical cuvette (diameter: 2.5 cm) were customized and placed at the center of the standard integrating sphere (diameter: 150 mm) of the PE950 spectrophotometer. Colonies were gently introduced into the cuvette using a cell and tissue culture flask (Jet BIOFIL, Ltd.) tilted at an angle greater than 90°, enabling the colonies to slide in slowly and minimizing the risk of structural disruption. Visual inspections were performed before and after each measurement. Any samples exhibiting visible damage were discarded. To minimize potential errors resulting from multiple scattering, a series of samples ($N = 3$–10) with gradient concentrations were prepared for each strain [34,37]. The absorption coefficients of the intact colonies (hereafter also denoted as a_{c_w}) were then determined from the optical density (OD_s) as follows [34],

$$a_{c\_w}(\lambda) = 2.303 \times OD_S(\lambda)/L \tag{2}$$

Here, L denotes the cuvette pathlength of 0.04 m.

2.2.2. Scattering and backscattering

The total scattering coefficient $b(\lambda)$ can be calculated indirectly as the difference between the beam attenuation coefficient $c(\lambda)$ and the absorption coefficient $a(\lambda)$, following the principle of inherent optical properties [34,36–37]. The beam attenuation coefficients $c(\lambda)$ can typically be measured by determining beam transmittance using a spectrophotometer [38–41]. Here, we modified the approach described by Tao et al. [42] by customizing a cuvette holder and an additional cuvette to cover the front port of the detector, and reducing the front port angle to approximately 0.23°. The dilution method [34,37] was used to minimize multiple scattering errors, which involves simultaneous measurement of the absorption coefficients $a(\lambda)$ and beam attenuation coefficients $c(\lambda)$ across a series of samples ($N = 3$-9) with gradient concentrations using a PE850 (for attenuation) and a PE950 (for absorption) spectrophotometer. The colony samples were handled using the same procedure as that used in the CIS measurements described in Section 2.2.1. Measurements of $c(\lambda)$ and $a(\lambda)$ were completed for the same sample within ±10 min. The calculation of $c(\lambda)$ is identical to that of $a(\lambda)$ [34]:

$$c(\lambda) = 2.303 \times OD_S(\lambda)/L \tag{3}$$

Here, L (the cuvette pathlength) is 0.1 m.

To assess the reliability of this approach, we measured standard particles from Thermo Scientific (mean diameter: 2.020 ± 0.015 µm; microsphere composition: polystyrene) and used Mie theory to simulate their spectral scattering coefficients. It was found that the theoretical scattering spectrum from the Mie simulation is in good agreement with the measured results (Fig. 3(a)), with only a slight discrepancy in the 400–420 nm range.

Subsequently, we also followed the scheme of Tao et al. [34] for measuring backscattering properties. Measurements were performed using a PE850 spectrophotometer equipped with an integrating sphere. A cuvette platform and a 14-cm-length reflectance cover of the integrating sphere (Fig. S1 in Supplement 1) were customized by Anhui Institute of Optics and Mechanics (Chinese Academy of Sciences). A correction for front-end interference from the quartz cuvette was applied by measuring both the sample and its 0.2 µm filtrate, with the final sample signal obtained by subtracting the filtrate measurement. Back-end interference is mitigated by placing a piece of low-reflectivity black aluminum foil (Thorlabs, Inc.) on the back end of the quartz cuvette during measurements. In addition, the cuvette was positioned at the exit port of the integrating sphere, where a monochromatic beam passed through it. This setup allowed the detector to capture the light backscattered by the suspension sample. A standard Spectralon plaque with a

Optics EXPRESS

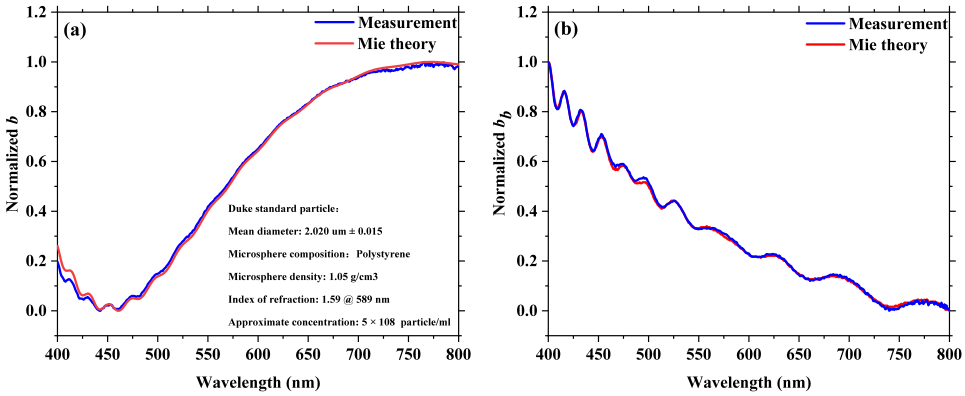

Fig. 3. Scattering (a) and backscattering coefficients (b) of standard particles, with the blue curve representing measured data and the red curve representing simulated data based on Mie theory.

nominal reflectance of 99.9% was used to measure the incident flux, with a 10-cm-pathlength sample cuvette. The ratio of the backscattered to incident flux ($R(\lambda)$) was then obtained and used to calculate the backscattering coefficient (b_b, m^{-1}) according to Eq. (4) as follows [34]:

$$R(\lambda) = 1 - \exp(-k \times b_b(\lambda) \times X) \tag{4}$$

Here, X denotes the length of the scattering volume [43], approximately taken as 0.1 m based on the cuvette length [34], also, k was set to 1. As with the scattering measurements, we used standard particles and Mie simulations to assess the reliability of the entire approach for backscattering coefficient measurements. Note that a cubic polynomial fitting process was involved in the Mie simulation [44]. The results, presented in Fig. 3(b), indicate excellent agreement between the measured and simulated $b_b(\lambda)$ spectra.

2.2.3. Other measurements and data processing

Chlorophyll *a* concentrations (Chl-*a*, mg m^{-3}) were determined fluorometrically [45]. The pigments from filtered samples were extracted in 90% acetone at -20°C in the dark for 24 h. Pigment profiles were determined using an UltiMate 3000 high-performance liquid chromatography (HPLC) system following standard analytical procedures [46]. Briefly, samples (5–50 ml) were filtered onto Whatman GF/F filters (0.7 µm), frozen in liquid nitrogen, and stored at −80°C. Pigments were extracted with N, N-dimethylformamide at −20°C and analyzed using a C_8 column (100 × 4.6 mm, 3.5 µm). Quantification of pigments was confirmed using the standards manufactured by the Danish Hydraulic Institute, Water and Environment, Hørsholm, Denmark. In addition, the 2nd derivative was employed to analyze the spectra of the IOPs [47,48].

3. Results

3.1. Absorption

3.1.1. Advantages of CIS measurement over QFT for P. globosa colonies

Figure 2(b) shows the a_{ph} spectra of PG-*in-situ* (red curve) obtained in this study. It appears that these a_{ph} spectra deviate from those of a typical phytoplankton absorption spectrum, particularly in the short-wavelength region. Such deviations are likely due to errors associated with uneven sample distribution on the filter pad, in particular for large-colony samples, as well as pathlength amplification correction and other unknown factors, making the a_{ph} spectra measured from

Optics EXPRESS

QFT appear questionable. Nevertheless, for cultured colonies, particularly very small ones (< 3 mm), QFT appears to perform better, as illustrated in Fig. 11 of Li et al. [13] and Fig. 2 of Astoreca et al. [10]. This is because their outer envelopes are less tough and elastic compared to those of field-collected colonies. In contrast, CCMA-124, a free-living cell strain without a colony envelope, exhibits a typical phytoplankton absorption spectrum (blue curve), as it does not suffer from the issue of uneven sample distribution on the filter pad. In a word, using QFT, it is possible to obtain the absorption properties of *P. globosa* colonies and to estimate the respective contribution of the envelope, the internal cells and CDOM to the colony's absorption, albeit with higher uncertainties in the short bands; the results, however, does not represent the absorption of intact colonies, but rather that of broken colonies. This, in fact, is exactly why we require CIS measurements.

The a_{c_w} of the free-living cell sample (CCMA-124) measured using CIS (black curve) is shown in Fig. 4, and it is in good agreement with that from QFT measurements (black dotted curve). This consistency confirms the reliability of our customized CIS system, given that the CCMA-124 is not a colony sample and thus avoids the issues and errors associated with QFT measurements. Similarities in the spectral shapes of a_{c_w} between CIS and QFT measurements are also observed for cultured colonies (CCMA-115, 1 mm in diameter on average, blue curves); deviations in shorter-wavelengths (particularly 400-440 nm), however, are evident, likely arising from absorption by unevenly distributed particulate detritus associated with broken envelopes (Fig. 2(a)). These results further indicate the reliability of our customized CIS system and its applicability to the absorption measurements for *P. globosa* colonies. On the other hand, the a_{c_w} of PG-*in-situ* (>20 mm in diameter) measured using CIS (red curve) differs substantially from that obtained via QFT (red dotted curve). This is most probably due to the issues associated with QFT measurements as mentioned above, in particular the severely unevenly distributed filter pad caused by the tough and elastic outer envelopes specific to field-collected colony samples (Fig. 2(a)). Interestingly, the a_{c_w} of PG-*in-situ* measured using CIS (red curve) closely matches that of the free-living cell sample CCMA-124 (black curve) in terms of spectral shapes.

Taken together, our customized CIS system appears capable of obtaining reliable absorption properties of intact *P. globosa* colonies, while absorption measurements via QFT yield results that are associated with higher uncertainties. Most importantly, CIS is currently the only method that enables measurement of *P. globosa* colonies in their intact state, a critical capability for accurate bio-optical modeling of its blooms.

3.1.2. Absorption properties of P. globosa colonies measured by CIS

Next, the absorption properties of *P. globosa* colonies were characterized based on the results measured by CIS. As described above, the absorption of large colony sample PG-*in-situ* and the free cell sample CCMA-124 closely match with each other in terms of spectral shape (Fig. 4). Besides the strains of PG-*in-siu* and CCMA-124, the left four *P. globosa* strains with colonies consistently show similar absorption feature measured using CIS, despite the colonies differing by an order of magnitude in size (see exemplar curves in Fig. 5(a), and all measured curves in Fig. S2a of Supplement 1). To enable direct comparison with the North Sea lab-cultured sample [10], the absorption coefficients (400–750 nm) for the six China Seas strains were normalized to a range of 0–2 by following Astoreca et al. [10]. It is obvious that all strains (six of the China seas and one of the North Sea) showed enhanced absorption in the range of 455–475 nm. This is attributed to Chl-c_3 prominent in *P. globosa*, which is consistent with findings in previous studies of *P. globosa* in the North Sea [10–11]. HPLC analysis of the six China Seas strains confirmed the presence of Chl-c_3 (Fig. 6). Nevertheless, this enhancement appeared at 465 nm for the free-living cell sample (CCMA-124) and shifted to 468–472 nm for all other strains with colonies, including the North Sea strain (PG-11), as indicated in the second derivative spectra (Fig. 5(c) & d). In addition, all six strains identified six major absorption maxima at roughly the

Optics EXPRESS

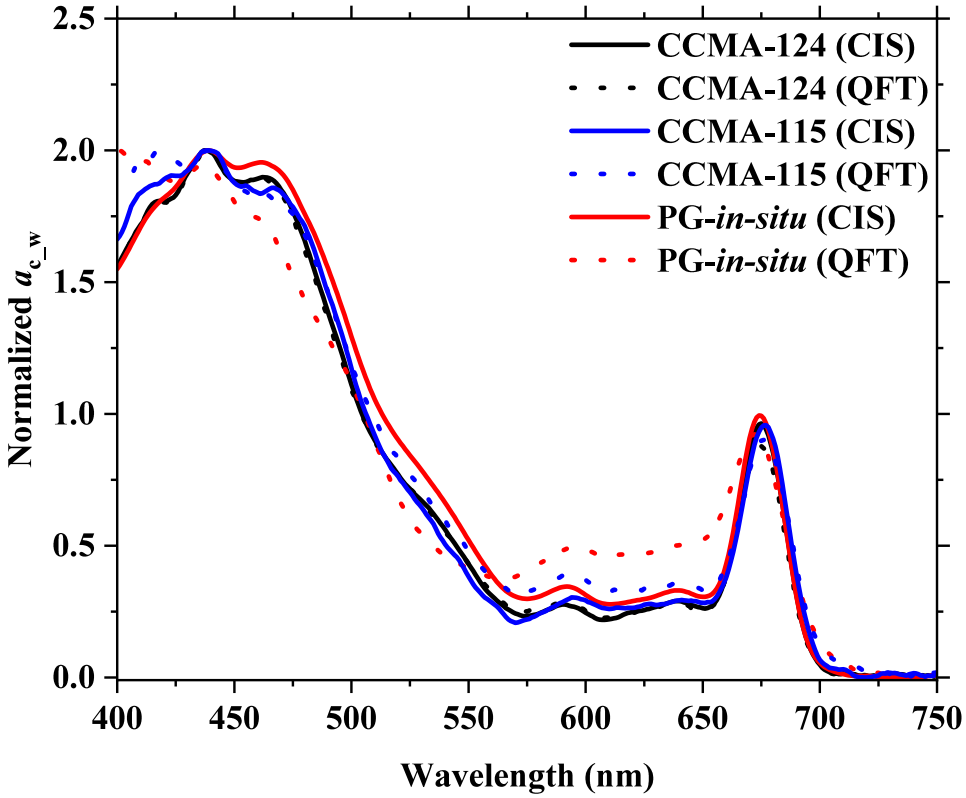

Fig. 4. The absorption coefficient of *P. globosa* colonies (a_{c_w}) measured via CIS (solid curve) compared to that measured via QFT (dotted curve), normalized to a range of 0-2; black: CCMA-124 (free-living cells), blue: CCMA-115 (tiny cultured colony, 1 mm in diameter), and red: PG-*in-situ* (large field collected colony, 25 mm in diameter).

same bands as those observed in the North Sea [10]. In summary, gelatinous colonies, regardless of their size, exhibit a dominant pigment absorption feature (~440 nm and ~675 nm for Chl-*a*, and ~455–475 nm for Chl-c_3). It appears that the envelopes and the CDOM contained in the intercolonial fluid make a negligible contribution to the light absorption of the colonies in the spectral range of 400-750 nm.

Interestingly, although the envelopes and the internal CDOM appear to make only a very minor contribution to the light absorption of the colonies, we found that the colonial structure itself does contribute. Ten sample groups of the strain PG-*in-situ* were tested. Each sample was measured twice using the CIS, first for its original form (intact colonies) and then for its physically broken form. All ten intact colony samples consistently exhibit a substantially higher chlorophyll-specific absorption coefficient ($a^*_{c\_w}$) than their corresponding broken samples, with results at MODIS bands listed in Table 2. Figure 7 presents the results of their mean $a^*_{c\_w}$ plus one standard deviation, clearly illustrating the reduced light absorption associated with the disruption of colony structure. Also, it further highlights that it is very important to use approaches such as the CIS proposed in this study to perform absorption measurements of colonies in their intact form.

Optics EXPRESS

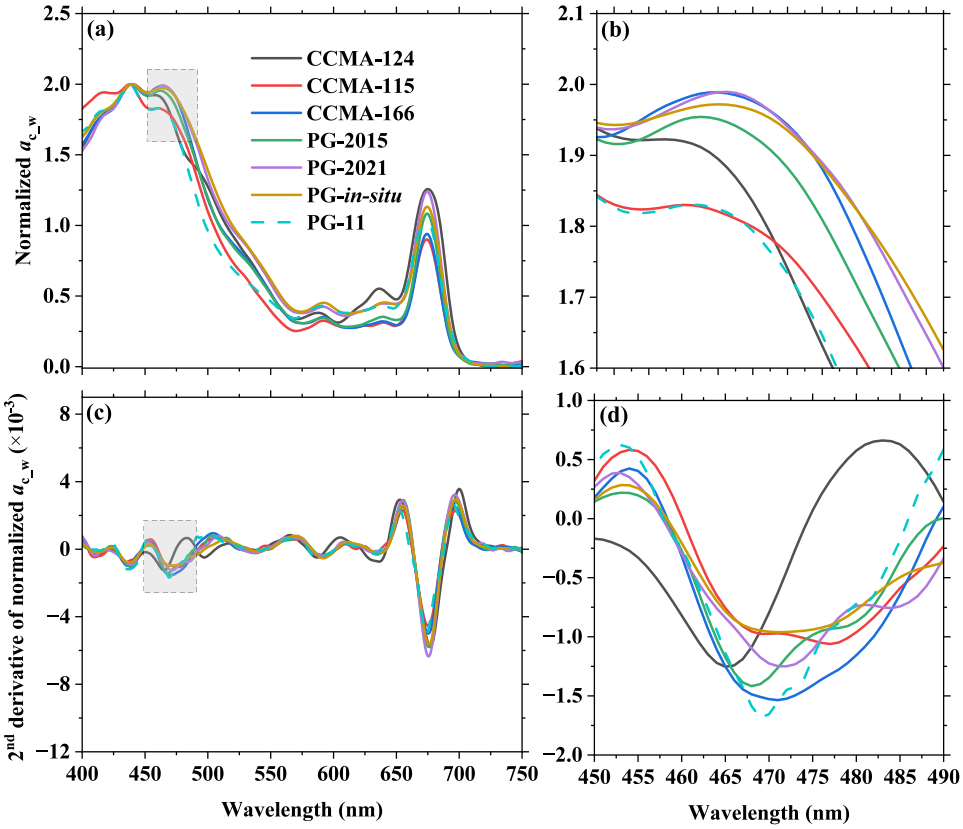

Fig. 5. (a) Exemplar absorption (a_{c_w}) spectra of six *P. globosa* strains isolated from China Seas, with the North Sea strain (PG-11) included for comparison; all were normalized to a range of 0-2 to enable better inter-strain comparison; (b) Zooming in the range of 450 nm to 490 nm in the grey region of (a); (c) Second-derivative of normalized a_{c_w}; (d) Zooming in the range of 450 nm to 490 nm in the grey region of (c).

Table 2. Statistics of chlorophyll-specific absorption coefficient ($a^*_{c\_w}$) of PG-*in-situ* ($N = 10$) at MODIS bands

Statistics / Wavelength / Colonies	Mean ± SD		Range	
	Intact colonies	Broken colonies	Intact colonies	Broken colonies
412 nm	0.045 ± 0.012	0.036 ± 0.009	0.027~0.060	0.021~0.048
443 nm	0.052 ± 0.015	0.042 ± 0.011	0.031~0.070	0.023~0.056
469 nm	0.051 ± 0.015	0.041 ± 0.011	0.030~0.068	0.022~0.056
488 nm	0.043 ± 0.012	0.035 ± 0.009	0.026~0.056	0.019~0.047
531 nm	0.023 ± 0.006	0.018 ± 0.004	0.014~0.029	0.011~0.024
547 nm	0.017 ± 0.004	0.013 ± 0.003	0.010~0.022	0.009~0.018
555 nm	0.014 ± 0.003	0.011 ± 0.002	0.008~0.018	0.008~0.015
645 nm	0.011 ± 0.003	0.008 ± 0.002	0.007~0.015	0.006~0.011
667 nm	0.024 ± 0.005	0.018 ± 0.004	0.015~0.031	0.013~0.025
678 nm	0.029 ± 0.007	0.022 ± 0.005	0.018~0.037	0.016~0.030

Optics EXPRESS

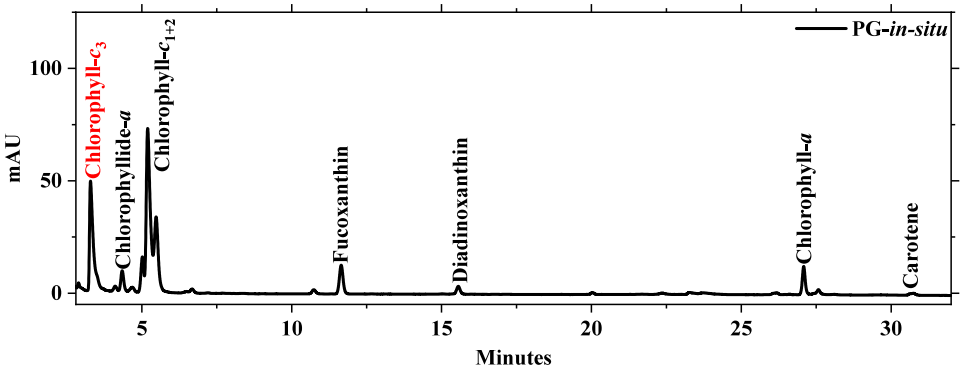

Fig. 6. Exemplar HPLC chromatogram depicting the pigment profile of the *P. globosa* strain PG-*in-situ*; Chl-c_3 is highlighted in red; data for five additional strains exhibit analogous profiles and are not depicted.

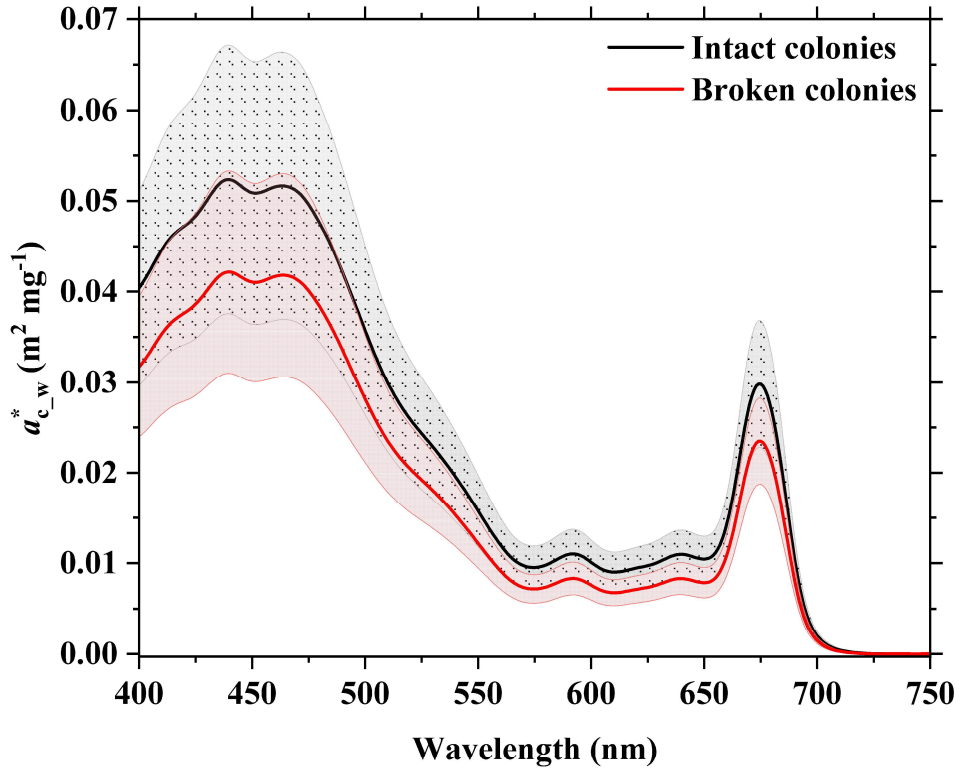

Fig. 7. Chlorophyll-specific absorption coefficient ($a^*_{c\_w}$) of PG-*in-situ* (field collected *P. globosa* colony sample) measured via CIS, with the black curve representing mean $a^*_{c\_w}$ of intact colonies and the red curve representing mean $a^*_{c\_w}$ of broken colonies ($N = 10$); the dotted grey and red shadows correspond to one standard deviation of the two mean curves, respectively.

3.2. Scattering and backscattering

The exemplar b and b_b characteristics of the six strains of *P. globosa* are shown in Fig. 8, normalized by their mean value from 400 nm to 750 nm (see all measured b curves in Fig. S2b of

Optics EXPRESS

Supplement 1). The spectral shapes of b and b_b for the six strains of *P. globosa* are roughly inverse to those of the absorption. This phenomenon can be explained by Ketteler–Helmholtz's theory of anomalous dispersion and is in agreement with experimental results reported in previous studies [33,34,44]. Overall, the b and b_b spectra of all *P. globosa* strains show approximately similar patterns, while subtle differences also exhibit; for example, the spectrum of CCMA-124 exhibits peaks and troughs of greater amplitude than those of the other strains (Fig. 8). These differences possibly arise from variations in the refractive index among different strains of *P. globosa* [43,49]. It appears that although the colonies are composed of extracellular polysaccharides that may affect scattering and backscattering, their b and b_b spectra are still generally consistent with the characteristics of free-living cells.

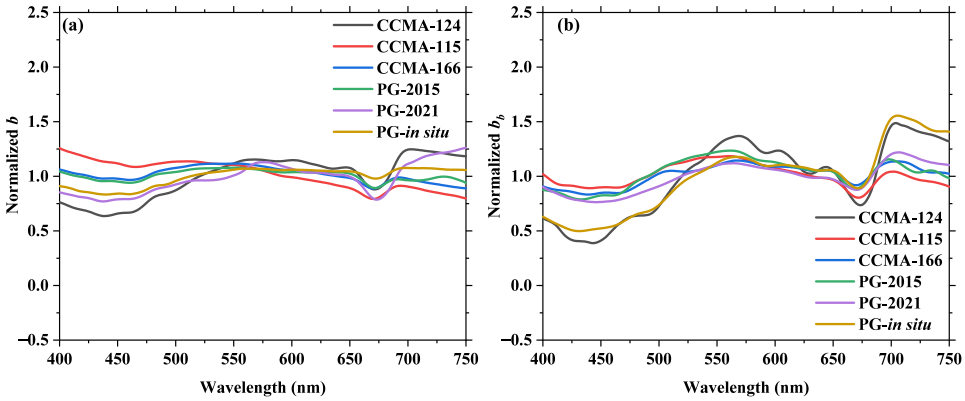

Fig. 8. Exemplar scattering (a) and backscattering coefficients (b) of six *P. globosa* strains, normalized by their mean values in the 400 -750 nm range.

4. Discussion

The above results demonstrate that the IOPs of intact *P. globosa* colonies isolated from China Seas, measured using optimized approaches, exhibit similarities to those of free cells, irrespective of size. Both the colony envelope and internal CDOM make only minor contributions to the light absorption and scattering of colonies in the spectral range of 400-750 nm. Additionally, the colony structure facilitates enhanced light absorption.

Then why do the colony envelope and the internal CDOM look almost transparent in the IOPs measurements? Based on QFT measurements for physically broken colonies (see the methods in Section 2), it was estimated that the absorption of the envelope at 443 nm was ~19.4%±5.5% of the a_{c_w} on average ($N = 26$), while the mean absorption of CDOM at 443 nm was ~5.5%±2.6% of a_{c_w} ($N = 26$). Although these data contain uncertainties arising from unevenly distributed filter pads and other factors noted in Section 2, and we have known that the absorption of broken colonies is lower than that of intact colonies, they indicate that the absorption by pigments within *P. globosa* cells dominates the overall absorption of colonies in the spectral range of 400-750 nm. This explains why the absorption properties of intact colonies show no detectable signature of detrital particles or CDOM, despite the fact that the envelope consists of particulate detritus and the intracolonial fluid contains CDOM.

Furthermore, we followed Smith et al. [3] to directly sample the intracolonial fluid of PG-*in-situ* with 2 mL syringes fitted with small-gauge needles. The sample was separated into two paralleled sub-samples. One was for CDOM absorption measurements according to the Ocean Optics Protocols Version 2.0 [32], and the other was measured using CIS to get the absorption coefficients of cells and CDOM in combination. The obtained CDOM absorption at 443 nm is 0.24 m^{-1},

Optics EXPRESS

while the combined absorption coefficient at 443 nm is 2.71 m^{-1}. Owing to the difficulty in sampling, only one sample of intracolonial fluid was obtained. Nevertheless, this limited result further confirms that within the intracolonial fluid, the absorption of CDOM at 443 nm accounts for only ~9% of the total absorption at 443 nm from both cells and CDOM combined. The absorption by cells is indeed overwhelming.

Smith et al. [3] observed that, in their study on giant *P. globosa* colonies in Vietnamese waters, the concentration of DOC in intracolonial fluid was 25 times higher than in ambient waters. However, the extent to which the measured DOC in that study was colored remains unclear. Unfortunately, we did not measure ambient CDOM absorption, and thus cannot determine whether CDOM within colonies is concentrated to the same extent as DOC in our field study (Dapeng Bay, China).

On the other hand, previous studies suggest that the colony structure may enhance the storage of light energy [50,51], in addition to regulating buoyancy [52], storing nutrients [53], and facilitating more efficient carbon sequestration [3]. In detail, when light is abundant, the colony structure aids in storing energy and nutrients, which colonial cells can then utilize to support growth during nighttime or periods of light limitation; consequently, *P. globosa* colonies may possess a greater survival advantage in resource-limited environments and can develop into blooms more rapidly [50,51]. Our observation indeed confirms the previous notion that the colony structure enhances light storage, as evidenced by the decrease in light absorption upon colony disruption. The primary mechanism for light trapping within colonies is likely the enhanced multiple scattering resulting from their colonial architecture. The gelatinous sheath of intact colonies and the complex cell–matrix interfaces can generate pronounced internal scattering. Through multiple internal scattering, the effective optical pathlength of photons within the colony is increased, thereby enhancing the probability of light absorption by pigments, analogous to pathlength amplification in strongly scattering media [54]. When colonies are disrupted, this optical "trapping" effect is weakened, leading to a measurable decrease in absorption.

Furthermore, it is implied that giant colonies of *P. globosa* probably can be approximated as large particles with similar IOPs in reflectance models, based on our results that both the colony envelope and internal CDOM make only minor contributions to the light absorption and scattering of colonies. It may not be that simple, however, as the samples in the measurements are just a few colonies contained in a few mL of static liquids, but in the field the situation would be much more complicated. Therefore, the possibility of approximating giant colonies of *P. globosa* as large particles is to be explored, depending on data collection in well-designed field campaigns of *P. globosa* blooms, with concurrent field remote sensing reflectance and the IOPs of colonies, as well as the IOPs and environmental properties of ambient waters collected. These forthcoming field and modeling studies are crucial for advancing remote sensing algorithms for *P. globosa* from empirical methods toward a mechanistic framework for bloom detection and biomass estimation.

In addition, several issues remain unresolved and warrant further investigation. First, a methodological challenge arises from the rapid sinking of colonies, compromising sample homogeneity and potentially increasing uncertainties in the results. In order to reduce the potential errors, the whole procedure must be completed in minutes, making the measurements highly skill-demanding. On the other hand, the impacts of environmental factors such as different levels of temperature, salinity, light, and nutrients, as well as different growth stages, on the IOPs of colonies deserve further exploration. Also, only one strain collected *in situ* was investigated in this study, necessitating the continuous collection of natural strains in their colonial form.

5. Conclusion

By modifying existing measurement methods, we obtained reliable IOPs of intact *P. globosa* colonies for six strains isolated from China Seas, including *in situ* and cultured samples with

Optics EXPRESS

varying colony size (1 mm–25 mm) and morphologies. Based on our study, it is highly recommended to use CIS for absorption measurements of *P. globosa* in future studies, at least for giant colonies. Furthermore, our experimental data refute the hypothesis proposed earlier, which posited that the IOPs of intact colonies differ from those of free-living cells and that the colony structure has no impact on the IOPs of *P. globosa*. It is now established that the IOPs of giant *P. globosa* colonies, at least for those in the China Seas, exhibit spectral shapes similar to those of free-living *P. globosa* cells in the range of 400-750 nm, with colony structure nonetheless playing a meaningful role in light absorbance. In other words, despite the highly concentrated cells within colonies (ranging from thousands to millions per colony), the intracolonial fluid contains only small amounts of CDOM, and the mucous envelope does not act as a strong light absorber and scatterer; also, the colony structure is of great significance for IOPs.

These results greatly improved our understanding of the optical properties of *P. globosa*, particularly in the China Seas, where giant colonies form during blooms. The pigment-dominated absorption characteristics of colonies, along with the influence of colony structure on light capture, provide a critical baseline for developing bio-optical models specific to *P. globosa* blooms. More importantly, our findings highlight the potential for remote detection of *P. globosa* colonies using hyperspectral sensors, given that the key optical marker, i.e., Chl-c_3 absorption, remains conserved regardless of colony size. Greater efforts dedicated to field-based optical investigations, encompassing both IOPs and apparent optical properties specific to colonies, alongside optical and biogeochemical properties of ambient waters, are certainly warranted. Only through enhanced *in situ* observations can bio-optical models specific to *P. globosa* blooms featuring giant colonies be developed, thereby facilitating the refinement of remote sensing algorithms for *P. globosa* blooms in optically complex coastal waters.

In summary, this study underscores the importance of preserving colony integrity in optical measurements and provides a foundation for improving the accuracy of remote sensing techniques for *P. globosa* blooms, including both detection and biomass estimation, with implications for ecological management and climate-related biogeochemical studies.

Funding. the Chinese Ministry of Science and Technology through the National Key Research and Development Program of China (2023YFC3107603); Basic Research Program of Jiangsu Province (BK20251055); National Natural Science Foundation of China (42506210).

Disclosures. The authors declare no conflicts of interest.

Data availability. The data presented in this study are available upon request from the corresponding authors.

Supplemental document. See Supplement 1 for supporting content.

References

1. V. Schoemann, S. Becquevort, J. Stefels, *et al.*, "*Phaeocystis* blooms in the global ocean and their controlling mechanisms: a review," J. Sea Res. **53**(1-2), 43–66 (2005).
2. R. Riegman and W. Van Boekel, "The ecophysiology of *Phaeocystis globosa*: a review," J. Sea Res. **35**(4), 235–242 (1996).
3. W. O. Smith, X. Liu, K. W. Tang, *et al.*, "Giantism and its role in the harmful algal bloom species *Phaeocystis globosa*," Deep Sea Res., Part II **101**, 95–106 (2014).
4. P. P. Shen, Y. Z. Qi, and L. J. Ou, "*Phaeocystis globosa* in coastal China: taxonomy, distribution, and its blooms," Marine Sciences **42**(3), 146 (2018).
5. P. P. Shen and Y. Z. Qi, "Research Progress on species diversity and distribution of the genus *Phaeocystis*," Harmful Algae **107**(1), 102057 (2021).
6. R. Astoreca, V. Rousseau, K. Ruddick, *et al.*, "Development and application of an algorithm for detecting *Phaeocystis globosa* blooms in the Case 2 Southern North Sea waters," J. Plankton Res **31**(3), 287–300 (2008).
7. B. Lubac, H. Loisel, N. Guiselin, *et al.*, "Hyperspectral and multispectral ocean color inversions to detect *Phaeocystis globosa* blooms in coastal waters," J. Geophys. Res. **113** (2008).
8. X. Li, S. Shang, Z. Lee, *et al.*, "Detection and Biomass Estimation of *Phaeocystis globosa* Blooms off Southern China From UAV-Based Hyperspectral Measurements," IEEE Trans. Geosci. Remote Sensing **60**, 4200513 (2022).
9. L. Peperzak and M. Poelman, "Mass mussel mortality in The Netherlands after a bloom of *Phaeocystis globosa* (Prymnesiophyceae)," J. Sea Res. **60**(3), 220–222 (2008).

Optics EXPRESS

10. Y. Z. Qi, J. F. Chen, Z. H. Wang, *et al.*, "Some observations on harmful algal bloom (HAB) events along the coast of Guangdong, southern China in 1998," Hydrobiologia **512**(1-3), 209–214 (2004).
11. N. Spilmont, L. Denis, L. F. Artigas, *et al.*, "Impact of the *Phaeocystis globosa* spring bloom on the intertidal benthic compartment in the eastern English Channel: A synthesis," Mar. Pollut. Bull. **58**(1), 55–63 (2009).
12. X. N. Lv, Z. X. Wu, X. X. Song, *et al.*, "Nutritional strategy for the preferential uptake of NO_3^--N by *Phaeocystis globosa*," Hydrobiologia **846**(1), 109–122 (2019).
13. Z. M. Yu, K. Wang, X. H. Cao, *et al.*, "Feasibility and Implementation of the Modified Clay Technique in Control of Phaeocytstis globosa Blooms in the Water-Intake Area of the Fangchenggang Nuclear Power Plant," in *International Conference on Nuclear Engineering* (American Society of Mechanical Engineers 2017), p. V003T013A015.
14. J. Chen, N. Xu, T. Jiang, *et al.*, "A report of *Phaeocystis globosa* bloom in coastal water of Southeast China," Journal of Jinan University Natural Science **20**(2), 124–129 (1999).
15. K. Wang, B. H. Chen, Y. H. Gao, *et al.*, "Harmful algal blooms caused by *Phaeocystis globosa* from 1997 to 2018 in Chinese coastal waters," Mar. Pollut. Bull. **173**, 112949 (2021).
16. J. X. Wang, F. Z. Kong, Z. F. Chen, *et al.*, "Characterization of pigment composition of six strains of *Phaeocystis globosa*," Oeanologia et Limnologia Sinica **50**(4), 611–620 (2019).
17. Z. J. Kang, B. Yang, J. X. Lai, *et al.*, "*Phaeocystis globosa* Bloom Monitoring: Based on *P. globosa* Induced Seawater Viscosity Modification Adjacent to a Nuclear Power Plant in Qinzhou Bay, China," J. Ocean Univ. China **19**(5), 1207–1220 (2020).
18. N. Guiselin, L. Courcot, L. F. Artigas, *et al.*, "An optimised protocol to prepare *Phaeocystis globosa* morphotypes for scanning electron microscopy observation," J. Microbiol. Methods **77**(1), 119–123 (2009).
19. H. Y. Song, F. Liu, Z. L. Li, *et al.*, "Development of a high-resolution molecular marker for tracking *Phaeocystis globosa* genetic diversity through comparative analysis of chloroplast genomes," Harmful Algae **99**, 101911 (2020).
20. A. A. Kurekin, P. I. Miller, and H. J. Van der Woerd, "Satellite discrimination of *Karenia mikimotoi* and *Phaeocystis* harmful algal blooms in European coastal waters: Merged classification of ocean colour data," Harmful Algae **33**, 55 (2014).
21. H. Lavigne, K. Ruddick, and Q. Vanhellemont, "Monitoring of high biomass *Phaeocystis globosa* blooms in the Southern North Sea by in-situ and future spaceborne hyperspectral radiometry," Remote Sens Environ **282**, 113270 (2022).
22. H. Chen, H. Yao, P. Liao, *et al.*, "Prediction of abnormal proliferation risk of *Phaeocystis globosa* based on correlation mining of PC concentration indicator and meteorological factors along Qinzhou Bay, Guangxi," J. Sea Res. **192**, 102365 (2023).
23. D. Li, Y. Xue, Q. Song, *et al.*, "First report on large-scale *Phaeocystis globosa* bloom in the southern Yellow Sea, China," Front. Mar. Sci. **9**, 880984 (2022).
24. J. Li, J. Lai, G. Xu, *et al.*, "Detecting the *Phaeocystis globosa* bloom and characterizing its bloom condition in the northern Beibu Gulf using MODIS measurements," Mar. Pollut. Bull. **209**, 117273 (2024).
25. G. Neukermans, H. Loisel, X. Meriaux, *et al.*, "In-situ variability of mass-specific beam attenuation and backscattering of marine particles concerning particle size, density, and composition," Limnol. Oceanogr. **57**(1), 124–144 (2012).
26. C. S. Yentsch, "Measurement of Visible light absorption by particulate matter in the ocean," Limnol. Oceanogr. **7**(2), 207–217 (1962).
27. S. Tassan and G. M. Ferrari, "An alternative approach to absorption measurements of aquatic particles retained on filters," Limnol. Oceanogr. **40**(8), 1358–1368 (1995).
28. P. G. Verity, C. P. D. Brussaard, J. C. Nejstgaard, *et al.*, "Current understanding of *Phaeocystis* ecology and biogeochemistry, and perspectives for future research," Biogeochemistry **83**(1-3), 311–330 (2007).
29. X. D. Wang, J. J. Zheng, and Y. Wang, "Effects of Grazing on the Colony Formation in *Phaeocystis globosa*," Journal of Tropical Biology **5**(1), 20–24 (2014).
30. R. Röttgers and S. Gehnke, "Measurement of light absorption by aquatic particles: improvement of the quantitative filter technique by use of an integrating sphere approach," Appl. Opt. **51**(9), 1336–1351 (2012).
31. A. R. Neeley, A. Mannino, E. Boss, *et al.*, "Ocean Optics & Biogeochemistry Protocols for Satellite Ocean Colour Sensor Validation," *International Ocean Colour Coordinating Group (IOCCG) in collaboration with National Aeronautics and Space Administration (NASA). Volume 1: Inherent Optical Property Measurements and Protocols: Absorption Coefficient.* (2018).
32. B. G. Mitchell, A. Bricaud, and K. Carder, "Determination of spectral absorption coefficients of particles, dissolved material and phytoplankton for discrete water samples," in *Ocean Optics Protocols For Satellite Ocean Color Sensor Validation, Revision 2*, eds. G. S. Fargion and J. L. Mueller, eds. (Greenbelt, Maryland: NASA Goddard Space Flight Center, 2000), pp. 125–153.
33. R. Röttgers, C. Hase, and R. Doerffer, "Determination of the particulate absorption of microalgae using a point-source integrating-cavity absorption meter: verification with a photometric technique, improvements for pigment bleaching, and correction for chlorophyll fluorescence," Limnol. Oceanogr.:Methods **5**(1), 1–12 (2007).
34. B. Tao, Z. Mao, D. Pan, *et al.*, "Influence of bio-optical parameter variability on the reflectance peak position in the red band of algal bloom waters," Ecol Inform **16**, 17–24 (2013).
35. N. B. Nelson and B. B. Prezelin, "Calibration of an Integrating Sphere for Determining the Absorption-Coefficient of Scattering Suspensions," Appl. Opt. **32**(33), 6710–6717 (1993).

Optics EXPRESS

36. A. Bricaud and A. Morel, "Light Attenuation and Scattering by Phytoplanktonic Cells - a Theoretical Modeling," Appl. Opt. **25**(4), 571–580 (1986).
37. A. Bricaud, A. L. Bedhomme, and A. Morel, "Optical properties of diverse phytoplanktonic species: experimental results and theoretical interpretation," J. Plankton Res. **10**(5), 851–873 (1988).
38. B. Tao, Z. Mao, H. Lei, *et al.*, "A semianalytical MERIS green-red band algorithm for identifying phytoplankton bloom types in the East China Sea," J Geophys. Res. Oceans **122**(3), 1772–1788 (2017).
39. B. Tao, Z. Mao, H. Lei, *et al.*, "A novel method for discriminating *Prorocentrum donghaiense* from diatom blooms in the East China Sea using MODIS measurements," Remote Sensing of Environment **158**, 267–280 (2015).
40. Y. L. Zhang, M. L. Liu, B. Q. Qin, *et al.*, "Modeling Remote-Sensing Reflectance and Retrieving Chlorphyll-*a* Concentration in Extremely Turbid Case-2 Waters (Lake Taihu, China)," IEEE Trans. Geosci. Remote Sensing **47**(7), 1937–1948 (2009).
41. S. G. H. Simis, M. Tijdens, H. L. Hoogveld, *et al.*, "Optical signatures of the filamentous cyanobacterium *Leptolyngbya boryan*a during mass viral lysis," Limnol. Oceanogr. **52**(1), 184–197 (2007).
42. B. Tao, D. Pan, Z. Mao, *et al.*, "Optical detection of *Prorocentrum donghaiense* blooms based on multispectral reflectance," Acta Oceanol. Sin. **32**(10), 48–56 (2013).
43. A. Bricaud, A. Morel, and L. Prieur, "Optical-Efficiency Factors of Some Phytoplankters," Limnol. Oceanogr. **28**(5), 816–832 (1983).
44. Y. Huang, M. Huang, Q. Song, *et al.*, "Study on the Backscattering Coefficient of Petroleum Polluted Waters with Multi-Angle Measurement," Journal of ocean Technology **36**, 7–13 (2017).
45. R. Parsons, "Discussion of spectrophotometric determination of marine plant pigments, with revised equation for ascertaining chlorophylls and carotenoids," J. Mar. Res. **21**(3), 155–163 (1963).
46. C. R. Mendes, P. Cartaxana, and V. Brotas, "HPLC determination of phytoplankton and microphytobenthos pigments: comparing resolution and sensitivity of a C_{18} and a C_8 method," Limnol. Oceanogr.: Methods **5**(10), 363–370 (2007).
47. Z. P. Lee, K. Carder, R. Arnone, *et al.*, "New band locations for remote sensors provide more accurate information about oceans," in SPIE Newsroom on December 11 (2007).
48. H. Y. Xi, M. Hieronymi, R. Rottgers, *et al.*, "Hyperspectral Differentiation of Phytoplankton Taxonomic Groups: A Comparison between Using Remote Sensing Reflectance and Absorption Spectra," Remote Sens. **7**(11), 14781–14805 (2015).
49. A. Morel and A. Bricaud, eds. *Theoretical results concerning the optics of phytoplankton, with special reference to remote sensing applications* (Plenum, 1981).
50. C. Lancelot, G. Billen, A. Sournia, *et al.*, "*Phaeocystis* blooms and nutrient enrichment in the continental coastal zones of the North Sea," Ambio (1987).
51. P. G. Verity, T. Villareal, and T. Smayda, "Ecological investigations of blooms of colonial *Phaeocystis pouchetti*—I. Abundance, biochemical composition, and metabolic rates," J Plankton Res **10**(2), 219–248 (1988).
52. X. Wang and K. W. Tang, "Buoyancy regulation in *Phaeocystis globosa* Scherffel colonies," Open Mar. Biol. J. **4**(1), 115–121 (2010).
53. M. Valero, S. Richerd, V. Perrot, *et al.*, "Evolution of alternation of haploid and diploid phases in life cycles," Trends Ecol. Evol. **7**(1), 25–29 (1992).
54. D. Mobley, *Light and Water: Radiative Transfer in Natural Waters*, Academic Press (1994).